EUROPEAN FUSION DEVELOPMENT AGREEMENT

EFDA–JET–PR(02)16

F. Crisanti, P.J. Lomas, O. Tudisco, A. Becoulet, M. Becoulet, L. Bertalot, T. Bolzonella, G. Bracco, M. de Benedetti, B. Esposito, C. Giroud, N.C. Hawkes, T.C. Hender, O.N. Jarvis, E. Joffrin, D. Pacella, V. Riccardo, F. Rimini, K.D. Lawson and contributors to the EFDA-JET workprogramme

Role of Plasma Shaping in ITB Experiments on JET

Tritium Removal from JET and TFTR Tiles by a Scanning Laser

F. Crisanti[1], P.J. Lomas[2], O. Tudisco[1], A. Becoulet[3], M. Becoulet[3], L. Bertalot[1], T. Bolzonella[4], G. Bracco[1], M. de Benedetti[1], B. Esposito[1], C. Giroud[3], N.C. Hawkes[2], T.C. Hender[2], O.N. Jarvis[2], E. Joffrin[3], D. Pacella[1], V. Riccardo[2], F. Rimini[3], K.D. Zastrow[2] and contributors to the EFDA-JET workprogramme*

[1]Associazione EURATOM-ENEA sulla Fusione, C.R. Frascati, Frascati, Italy
[2]UKAEA Fusion, Culham, JET Joint Undertaking, Abingdon, Oxon, OX14 4DB, UK
[3]Association EURATOM-CEA, CE de Cadarache, F-13108, St Paul lez Durance, France
[4]Associazione EURATOM-ENEA sulla Fusione, Consorzio, RFX, Padua, Italy

**See appendix of J. Pamela et al, Fusion Energy 2000 (Proc. 18th Int, Conf. on Fusion Energy, Sorrento 2000), IAEA, Vienna*

Preprint of Paper to be submitted for publication in
Plasma Physics and Controlled Fusion

ABSTRACT

A set of dedicated JET experiments is described where the plasma elongation (k) and triangularity (δ) were varied separately in order to study the influence of plasma magnetic topology on the Internal Transport Barrier (ITB). With low δ, type III ELMs were observed and ITBs readily generated. At the highest δ, large type I ELMs and ELM free phases were observed but, at best, only marginal ITBs. At fixed δ the increase of the elongation of internal magnetic surface seems to have a beneficial effect on the transport quality of the ITB.

INTRODUCTION

It is well known that plasma shaping plays an important role in the edge transport barrier regimes (H and VH modes). The magnetic topology is involved both in establishing the transport barrier and in the stability property of the pressure pedestal [1,2,3,4]. In principle these edge features and characterisations should not have strong direct influence on the properties of an Internal Transport Barrier (ITB). For instance, in a previous JET experimental campaign with different divertor geometry (MkIIA), ITB plasmas were obtained both in H and L mode [5].

With the JET gas box divertor (MkIIGB with septum), where the H mode power threshold appeared lower, it was quite difficult to achieve an ITB in L-mode plasmas. Therefore the Edge Localized Mode (ELM) activity became an issue. The cold pulse from large ELMs, particularly of type I, can perturb the ITB and strongly downgrade the transport properties [6] even for plasmas with weak shaping. However, since ITER is planning to work with highly triangular plasmas, it is important to explore in the present JET the interconnections between the edge stability properties (which depend upon the plasma shaping) and the internal transport behavior.

A more direct role for the plasma shaping can also be expected in the characterisation of the ITB itself. The internal magnetic topology is important both in the turbulence onset [7] and in the turbulence reduction mechanisms [8]. Normally the external shaping degrades going deeper in the plasma radius, however, by adjusting the plasma current profile, and hence the q profile, it is possible to vary (at fixed boundary shape) the internal flux surface topology.

Four different plasma shaping configurations have been planned and realised in JET experiments, changing both elongation and triangularity at fixed plasma current and fixed toroidal field. The variation in triangularity was sufficient to address the problems of operating in ITB configuration in the presence of large ELMs. Indeed for the most extreme shape, the ELMs were so large as to exceed the limits of the vertical stabilisation system and this made it difficult to obtain other than marginal ITBs in this case. Nevertheless some important features were observed: the usual increase of the local pressure gradient with the triangularity was found, [9, 10]. The stability properties of the edge pedestal are described and analysed in this paper. The elongation scan does not affect sensitively the operational scenario and in particular the ELM behaviour; this has allowed an investigation of the effect of the modifications of the magnetic topology due to elongation on the quality of the internal barriers. Preliminary studies show that the radial electric field depends on the internal magnetic surface topology. Finally, for this scan, a comparative transport analysis is presented.

EQUILIBRIUM CONFIGURATION

For a good exploration of the shaping parameters four different equilibrium configurations (Table 1) were planned:
a) High Triangularity, High Elongation (HD-HK);
b) High Triangularity, Low Elongation (HD-LK);
c) Low Triangularity, High Elongation (LD-HK);
d) Low Triangularity, Low Elongation (LD-LK)

[note 1]Many JET equilibria can be dialed up by name, including these, and for clarity it is convenient to retain these names. The convention is L for low, H for high, D for delta, K for kappa. Thus LD_LK indicates low δ low k, whereas HD_HK indicates high d high k.

In all the configurations the toroidal field (B_T = 2.6T) and the plasma current (I_p = 2.2 MA) were kept constant, therefore, as a consequence of the plasma shape variation, the safety factor qy changes over the range $q_{95\%} = 3.0 \div 3.4$. $q_{95\%}$ is the value of q_ψ at 95% of the flux function. As reference point, the elongation and the triangularity for the discharge #53521 are also reported. This discharge was the target for the experiments on steady state ITBs [11]. The realised equilibrium configurations are shown in Fig.1(a) (high triangularity, low and high elongation) and in Fig.1(b) (low triangularity, low and high elongation). In principle, higher triangularity than the extreme case shown should be possible on JET up to δ=0.55. However, the septum of the Gas Box divertor used in these experiments constrains such cases to even higher elongation and smaller minor radius where vertical stability becomes an issue. Already for HD_HK an ELM induced Vertical Displacement Event (VDE) occurred at the first large type I ELM in every case. For all four configurations the location of strike points and X-point was chosen to be broadly similar in order that divertor recycling plays a similar role. This is illustrated in more detail in Fig.2(a) for the elongation scan (κ=1.67-1.76) at low triangularity. In spite of this choice, as will be shown in the following section, the ELMs behaviour changed quite a lot between the different configurations.

As expected, the features characterising the plasma shaping (κ, δ) downgrade going towards the plasma centre; however in magnetic shear (s = r/q dq/dr) reversed configurations the lack of central current makes it possible to have more shaped internal flux surfaces [12]. This is shown in Fig.3 where the elongation of the internal flux surfaces is compared for two discharges with similar values of poloidal beta β_p, $q_{95\%}$, and edge elongation, but with different q_ψ profiles. The magnetic shear is positive all over the minor radius for the shot #52371 whilst it is negative in the central region for the shot #51970. It can be seen that the radial behavior of the elongation is strongly connected with the qy profile, so that the plasma internal magnetic topology can be varied, keeping fixed the boundary shape, by controlling the current profile. As a consequence, when comparing discharges with different boundary shaping, particular care must be paid to the radial behavior of qy to guarantee a similar internal magnetic topology [13]. The use of Lower Hybrid Current Drive (LHCD) during the plasma current rise made it possible to have a degree of current density profile control [11], therefore it was possible to get discharges with exactly the same shape of boundary, but with different shape of internal flux surfaces.

ELM BEHAVIOUR

Changing the shape of the last closed magnetic surface, at fixed total plasma current and toroidal magnetic field, obviously implies different edge safety factor q; moreover a different topology of the flux surfaces is intrinsically connected with different magnetic shear. The most important consequence of these points is that the plasma edge stability is strongly affected by any variation of the geometrical shaping [14].

The H mode threshold in JET experiments with the Gas Box divertor was lower than with the previous divertor (MkIIA); therefore the ITB experiments were almost always in the H mode regime. In particular in all the discharges with the standard shaping the pedestal pressure was such that ELMs, usually of type III, were present. In Fig.4 the typical D_α traces for the four configurations studied are shown. The configuration with lowest δ and κ, LD_LK (#52659 Fig.4(a)), was always characterised by the presence of type III ELMs, although the total injected power (typically 15MW) was higher than the expected threshold for the transition between Type III and Type I ELMs [6]. The configuration LD_HK usually exhibited type III ELMs (e.g. #52630 Fig.4(b)), though in 3 out of 8 pulses short ELM free phases (<100ms duration) were followed by a single type I ELM and a return to type III. For the two high triangularity cases longer ELM free phases (200-800ms duration) were followed by a large Type I ELM. In #52645 HD_HK (Fig.4(c)) the long ELM free phase was followed by an ELM so large that the vertical stabilisation system reached its current limit and a

Vertical Displacement Event (VDE) led to a major disruption Attempts to avoid this sequence of events by reducing the power and injecting an impurity gas (neon) were not successful. In #52624 HD_LK (Fig.4(d)), the discharge briefly returns to type III ELMs after the first type I ELM, and after the second type I ELM returns to and remains with type III ELMs and subsequently an ITB forms at about 5.5s. A similar behaviour was seen for 3 out of 5 shots employing this configuration, the remaining two shots suffered from ELM triggered VDEs. The occurrence of type I ELMs in both the high triangularity configurations indicates that the increase of triangularity has the effect of reducing the threshold for the type III to type I transition.

The edge Thomson Scattering diagnostic (LIDAR) was used to measure the pedestal plasma pressure. In Fig.5 these measurements are reported for different time slices of the two extreme configurations LD-LK and HD-HK. In particular for the first configuration, where the pedestal pressure and ELM behavior do not change, only a single time slice is shown (see the vertical line of Fig.4(a)); for the most extreme case the full time evolution is shown. The vertical lines on Fig.4(c) mark three different situations. For the first time slice the ELM behavior and the pedestal pressure Fig.5(b) are similar to the previous case. For the second time slice, type I ELMs are present and the pedestal pressure is higher Fig.5(c). Finally, an ELM free phase Fig.4(c) and strong pedestal pressure gradient appear Fig.5(d), and here the time slice is taken just before the giant ELM that leads to plasma disruption. The ideal ballooning stability has been analysed using the method of [15] for the discharges reported in Fig.5. The pressure gradients are replotted in the α-s space (Fig.6), where $a = 2m_0Rq^2(dp/dr)/B^2$. Both the quantities a and s are evaluated at the 95% flux surface. The actual Thomson Scattering measurements are performed in a region just above the X-point location. However, by using the flux surface geometry reconstructed by the equilibium code EFIT, the pressure measurements are transformed onto the outer midplane, where the pressure derivative is evaluated. The magnetic shear values are also taken from the EFIT output but do not take into account the local bootstrap current and its effect on the magnetic shear. However, this, in principle, should reduce the local magnetic shear. Some important features are immediately evident from the figure.

In both the discharges, when type III ELM activity is present the experimental α-s point is not too far from the left boundary of the first stability region. When the ELM amplitude increases and the frequency starts to reduce, i.e. during the type I phase, the α-s point moves inside the unstable region. Finally at the end of the ELM free phase the edge seems to be inside the second stability region. However, it should be borne in mind that large uncertainties in the experimental edge data could strongly modify the experimental points on the a-s plane and, via self-consistent bootstrap currents, the boundary of the stability region. Interestingly, [16] has shown that with the inclusion of edge bootstrap current, for similarly high triangularity but for fully relaxed internal current profiles, JET ELMy H modes approach the domain of second stability, but that access to unambiguous second stability is barred by medium n kink modes. The large and unambiguous increase in the edge pressure gradients presented in this paper is strongly indicative that similar physics applies in both cases.

SHAPING AND INTERNAL PLASMA FEATURES.

To explore the role of the internal magnetic surface topology on the plasma performance two approaches are presented; firstly, a statistical one to elucidate the general trends and, secondly, a more direct comparison of matched pairs of discharges where all input parameters, except the shaping, were comparable [17]. *a) Statistical approach.* The possible correlation between plasma shaping and plasma core confinement in the recent JET data has been explored statistically for discharges having hollow current profiles. In Fig.7 the ion temperature, at three different radial positions (r/a~0, 0.5, 0.9), is plotted versus the upper triangularity (note that the lower triangularity varies little). In the selected data the total power (Neutral Beam Injection +Ion Cyclotron Resonance

Heating, i.e. NBI + ICRH) varies between 12 and 16 MW. The solid symbols refer to discharges with high elongation ($k > 1.75$) and the open symbols refer to discharges with low elongation ($k < 1.75$). For discharges with high triangularity ($\delta > 0.3$), which tend to exhibit transient ELM free phases, all points on the plots are taken during such phases. It can be seen from Fig.7 that the effect of the triangularity is to increase the edge temperature (pedestal) and to decrease the central one giving rise to a broadening of the ion temperature profile. Although the ITB quality downgrades, the confinement factor H_{89} for these discharges actually increases with triangularity due to the increase of the pedestal. Strongly elongated (solid symbols) and weakly elongated (open symbols) discharges have the same behaviour, so that no dependence on elongation can be inferred from this plot.

As already noted, the change in the ELM activity with the shaping has been a major feature of the experiments and the data analysis reflects this point. At high triangularity the ELM triggered VDE precluded operation at high power. Furthermore, the increase of triangularity decreased the power threshold for transitions between type III and type I ELMs and consequently showed the type I ELM feature all the time. Sarazin has already shown for weakly shaped plasmas [6], that the energy loss associated with a strong type I ELM strongly affects the ITB behaviour. Finally the ELM free phase and the duration of this phase change with triangularity and power, so that any inference about the confinement from the triangularity scan is strongly affected by the ELM behaviour. Although we do not have a unique explanation for the negative trend of the central ion temperature with triangularity, it should be pointed out that this behaviour is qualitatively in agreement with the prediction of a gyro-fluid code [7] for the linear growth rate of Ion Temperature Gradient (ITG) driven turbulence. In fact, for high aspect ratio ($A \approx 6$) as on the inner flux surfaces, the linear growth rate gITG increases when triangularity rises from 0 to 0.4. A beneficial effect can be observed only at triangularity beyond this value but such as practically unattainable on JET internal magnetic surfaces. An analogous, but weaker, negative behavior is expected for the geodesic curvature with d, at the aspect ratio of the ITB radius, whilst in contrast, for the higher triangularity and lower aspect ratio near the edge a beneficial effect on the pedestal pressure is predicted [8].

In Fig.8 the ion temperature, at three different radial positions ($r/a \sim 0$, 0.5, 0.9), is plotted versus the plasma elongation for the same points of Fig 7. The open and full symbols refer respectively to $\delta < 0.3$ and $\delta > 0.3$. No clear dependence of the ion temperature on elongation is apparent at any radius. A decrease both of the geodesic curvature [8] and of the linear growth rate [7] is expected with increasing local plasma elongation, but such effects are not made manifest on this plot of experimental data. However, since there is a stronger dependence of the ITG linear growth rate on other parameters (especially magnetic shear) than on flux surface shaping, it is possible that the expected effects are obscured by the variations in these other parameters. This possibility is explored in the next paragraph.

b) Direct comparison of similar discharges. In order to compare discharges with different elongation but similar current diffusion, pairs of discharges were selected with identical time evolution of macroscopic parameters (I_p, P_{TOT} etc.). Two suitable pairs of discharges (#52656- #52664 and #52635- #52658) were identified. Figure 9 shows the time evolution of the main parameters of one pair (#52656 full line, #52664 dashed line). In both discharges the triangularity is low and the position of the X-point is almost the same (Fig.2(a)), and moreover they show the same type of ELM activity (Fig.2(b)) [18, 19]. The elongation of the two discharges range from $k = 1.65$ (#52664) to $k = 1.76$ (#52656). Note the differences in time evolution of central ion temperature and the JET ITB criterion ρ_{Ti}^* [20] in Fig.9(e) and Fig.9(f). $\rho_{Ti}^* = \rho_s / L_{Ti}$, where ρ_s is the local Larmor radius at the thermal sound velocity and L_{Ti} is the ion temperature gradient scale length. Conventionally a clear ITB exists when $\rho_{Ti}^* > 1.4 \times 10^{-2}$ marked by the horizontal line on Fig.9(e). The more elongated discharge #52656 develops the barrier earlier (i.e. at a lower power) while less elongated discharges develops the ITB only during the peak of the auxilliary heating. This is an

indication that the ITB power threshold is lower in discharges with more elongated internal flux surfaces and this is an indication of a lower linear growth rate for turbulence. In these discharges the neutron rate (Fig.9(d)) predominantly comes from beam-plasma interaction (80%) so that the higher ion temperature does not correspond to an equivalent increase of the neutron rate [21]. Figure 10(a-c) shows the ion temperature, the electron temperature and the electron density profiles for both pairs of selected shots; in Fig.10(d) the q_ψ profile (as obtained by EFIT constrained by MSE) for one pair is shown. The density and the q_ψ profiles are essentially the same for both pairs of discharges except that the edge density is slightly higher for #52658 compared with #52635. For both pairs the discharge with the higher elongation has higher ion temperature everywhere but most notably in the ITB. The electron temperature is slightly higher inside of the ITB region for the higher elongation case in each pair.

Using the transport code JETTO in interpretative mode, a power balance analysis for the two shots #52656 and #52664 has been performed. The total confinement time of the shot with higher elongation was, as expected, higher than that of the other discharge. The time evolution of the thermal conductivity for electrons (χ_e) and ions (χ_i) at fixed radius, R=3.4 m (close to the barrier foot), is shown in Fig.11, together with the radial electric field [11] E_r. During the phase of the temperature increase the most elongated discharge has a lower thermal conductivity, whilst it reaches more or less the same value during the stationary phase. As discussed before, the same behavior is seen on ρ_{Ti}*. Since this is a measure of the ion temperature gradient, it indicates clearly that the improvement in χ_i reflects the increase of ΔT_i. The same feature is present at all radii, showing that the increase of the temperature gradient is due to a reduction of the energy transport coefficient. The radial electric field, E_r (Fig.11(c)), is higher for the case with high elongation and remains higher throughout the heated phase. In both cases the electric field increases at the time of ITB formation, but this increase occurs earlier for the discharge with higher elongation. These observations are consistent with the hypothesis that the effect of magnetic topology on transport leads to an increased radial electric field and hence earlier turbulence suppression and ITB formation.

CONCLUSIONS.

Dedicated experiments have been performed on JET to elucidate the interrelations between plasma shaping and the ITB. In particular four different equilibrium configurations have been realised to explore the extreme combinations of elongation and triangularity. A clear trend of increasing pedestal pressure, and a change from type III to type I ELMs was observed with increasing triangularity. These effects dominate and restrict the opportunity to study the effects of triangularity on the ITB performance, although marginal ITBs have been obtained.However the edge stability properties have been analysed indicating that, during the ELM free phase, the plasma edge is in the second stability region (ignoring edge bootstrap currents). A comparison of the analysis presented here with an analysis of conventional ELMy H-modes at similar values of triangularity where possible bootstrap effects are explored suggests that both cases approach the second stable domain. The central ion temperature decreases with increasing triangularity (over the range explored here) indicating a negative effect of triangularity on ITB performance. This is consistent with the predictions of increased ITG linear growth rate or the increased geodesic curvature. Significantly higher values of triangularity would be required for the effect of geodesic curvature to become favourable. An alternative explanation of the negative trend with triangularity could be the increasingly destructive effect of the ELM perturbation on the ITB [6].

For the case of the elongation scan at low triangularity the ELMs remain type III at both low and high elongation. In the data as a whole, any trend with elongation is obscured by variations in input power, timing and in particular variations in q profile. It is therefore necessary to select carefully matched pairs of discharges at high and low elongation. In each pair the discharge with higher

elongation shows a stronger ITB with higher central electron and ion temperature, whereas the q profiles are very similar. In addition, the ion temperature is higher before ITB formation and the ITB forms earlier for the higher elongation cases. Transport analysis shows lower thermal conductivity and higher radial electric field at high elongation, and interestingly differences are apparent even before ITB formation. Models predict that the change in magnetic topology should reduce transport, thereby increasing the radial electric field and favouring turbulence suppression consistent with the observations.

Of course, given the limitations of the measurements and the indirect nature of the analysis, a definitive conclusion is not possible. This is, perhaps, the reason such an experiment has not previously been attempted. Nevertheless, the experiments presented here give strong support, albeit of a somewhat qualitative nature, to theoretical models of turbulence suppression and the role of magnetic topology.

ACKNOWLEDGEMENT.
This work was performed under the European Fusion Development Agreement.

REFERENCES.

[1]. Lao L.L, Ferron J.R, et al., 1999 Nucl. Fusion **39** 1785
[2]. Lao L.L, Kamada Y, et al., 2001 Nucl. Fusion **41** 295
[3]. Saibene G, Horton L.D, et al., 1999 Nucl. Fusion **39** 1133
[4]. Sartori R, et al., 1999 Europhys. Conf. Abstract **23J** 197
[5]. Gormezano C, 1999 Plasma Phys. And Contr. Fusion **41** B367
[6]. Sarazin Y, Becoulet M, et al., 2002, submitted to Plasma Phys. And Contr. Fusion
[7]. Waltz R.E and Miller R.L, 1999 Physics of Plasmas **6** 4265
[8]. Alladio F, Crisanti F, 1999 Physics of Plasmas, **6**, 2472
[9]. Osborne T.H, et al., 2000 Plasma Phys. And Contr. Fusion **42** A175
[10]. Wolf R.C, et al., 1999 Plasma Phys. And Contr. Fusion **41** B93
[11]. Crisanti F, Litaudon X, et al., 2002 Submitted to Physical Review Letter
[12]. Turnbull T.S, Taylor T.S, et al., 1998 Nucl. Fusion **38** 1467
[13]. Rice B.W., et al. 1997 Nucl. Fusion **37** 517
[14]. Bondeson A, Benda M, Persson M, 1997 Nucl. Fusion **37** 1419
[15]. Green J.M, Chance M S, 1981 Nucl. Fusion **21** 453
[16]. Huysmans G, 2001 9th European Fusion Physics Workshop, Saariselka, Finland, 2001.
[17]. Tudisco O. et al,2001 28th EPS, Madeira, 18-22 June 2001 (P2.013)
[18]. Sips A.C.C et al., 1999 26th EPS Conf., Maastricht, P1.027
[19]. Lomas P J, et al., 2001, 28th EPS Conf., Madeira P2.023
[20]. Tresset G. et al., 2001 to be published in Nucl. Fusion
[21]. Bertalot L, Jarvis, O.N, 2001 Private Communication

Table.1

	K	**<δ>**	**SHOT #**
HD-LK	1.65	0.35	52624
LD-HK	1.78	0.27	52630
HD-HK	1.80	0.46	52645
LD-LK	1.66	0.23	52664
Standard	1.67	0.20	53521

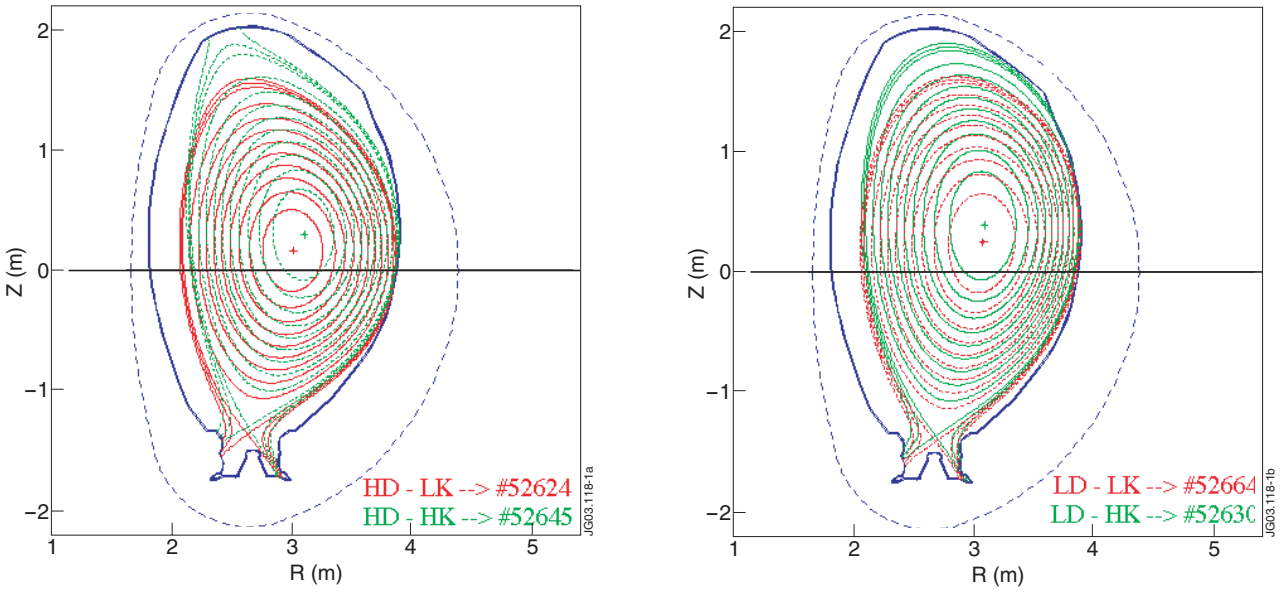

Fig.1: The realised equilibrium configurations. In fig.1(a) are shown the configurations at high triangularity and different elongation (in red HD-LK→ #52624; in green HD-HK→ #52645). In fig.1(b) are shown the configurations at low triangularity and different elongation (in red LD-LK→ #52664; in green LD-HK→ #52630).

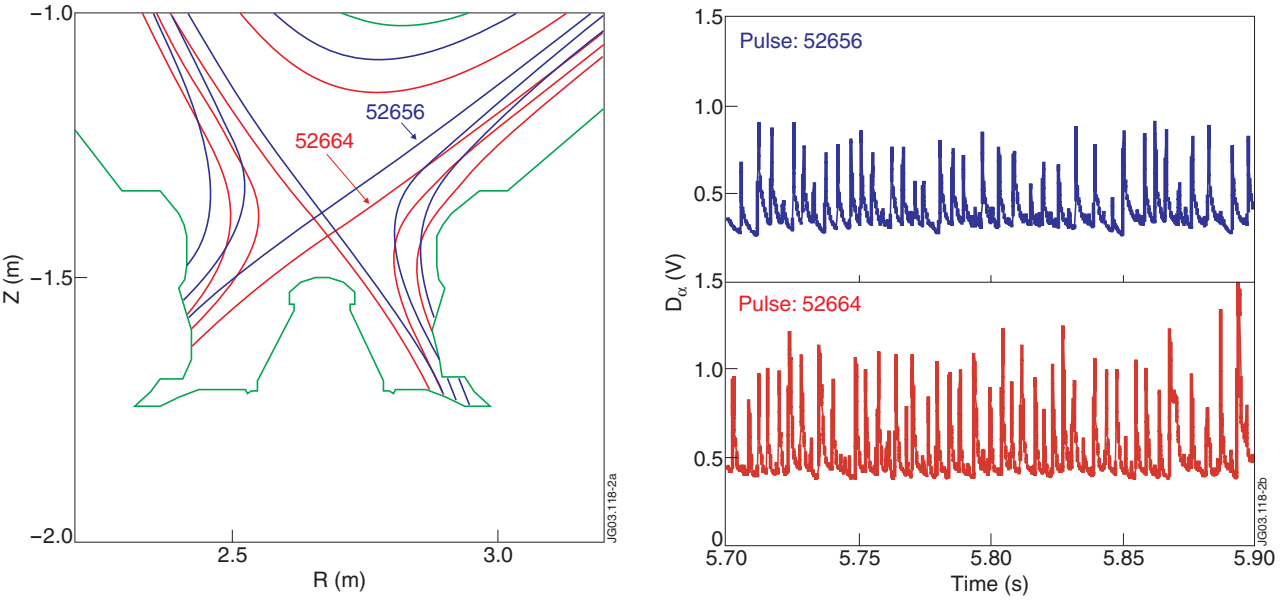

Fig.2: X point position (2(a)) and ELM behaviour (2(b)) for two discharges similar in all the parameters, but the elongation: #52656 (LD-HK); #52664 (LD-LK)

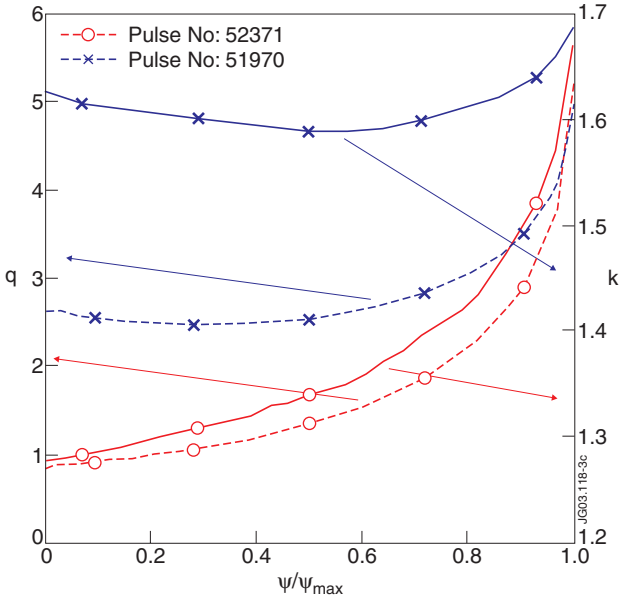

Fig.3: Flux surface elongation and q_ψ versus the plasma radius for two discharges with different current density profile: monotonic for pulse #52371 and reversed for pulse #51970

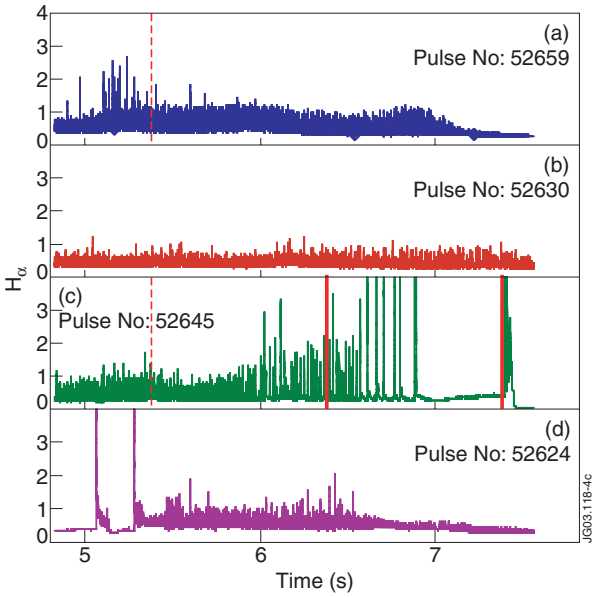

Fig.4: ELM behaviour for the four different configurations, a) #52659 (LD-LK); b) #52630 (LD-HK); c) #52645(HD-HK); and d) #52624 (HD-LK). The vertical lines indicate the times where the edge pressure has been measured (see Fig.5).

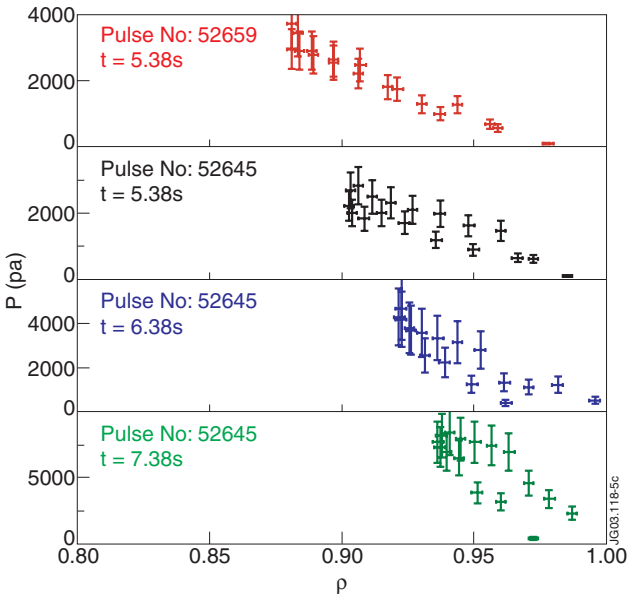

Fig.5: Edge plasma pressure measured by the Thomson scattering versus the normalized plasma radius for two elongated discharge but with low triangularity (#52659, LD-LK top box) and high triangularity (#52645, HD-HK). The times are marked by the vertical bars on Fig.4(a) and Fig.4(c).

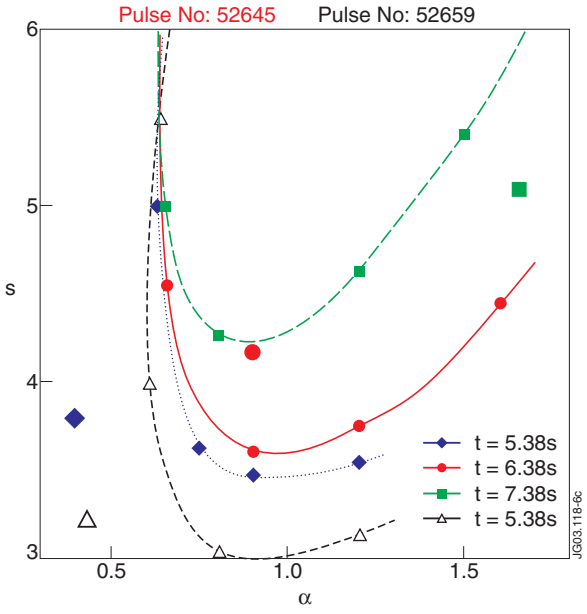

Fig.6: Position in the α-s plane of plasma edge for the shot #52645 (HD-HK) at three different times (filled symbols), with increasing plasma pressure, corresponding at different ELM behavior. The lines limit the stable-unstable regions and the large symbols indicate the experimental points. The discharge #53659 (LD-LK, open symbols), with ELMs type III is shown for comparison.

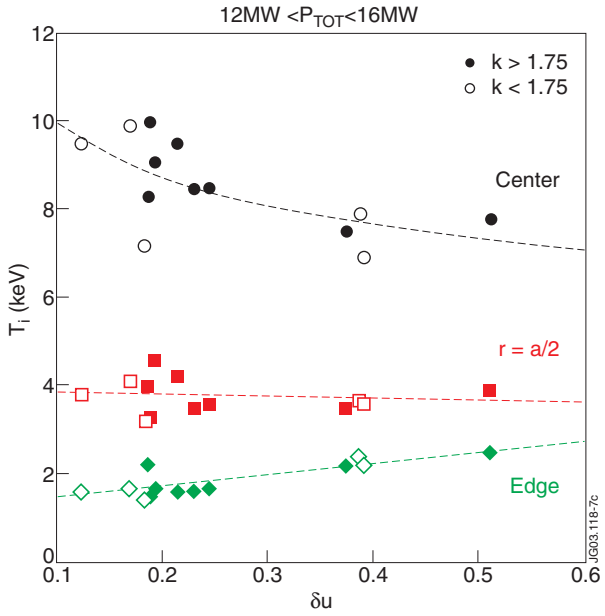

Fig.7: Ion temperature at three different plasma radius, versus the upper triangularity, for classes of elongation.

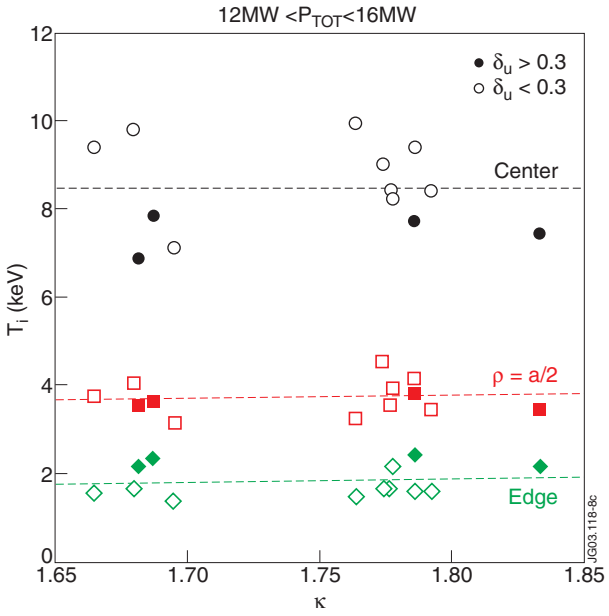

Fig.8: Ion temperature at three different plasma radius, versus elongation for two classes of triangularities.

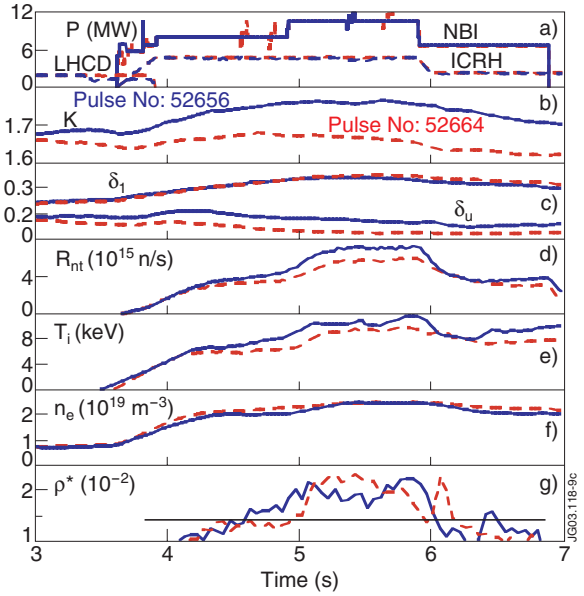

Fig.9: Time behavior for several plasma quantities for the discharges #52656 (LD-HK) and #52664 (LD-LK). a) NBI, ICRH and LHCD injected powers; b) plasma elongation; c) upper triangularity; d) neutron yield; e) ion temperature; f) line average electron density; g) ρ.*

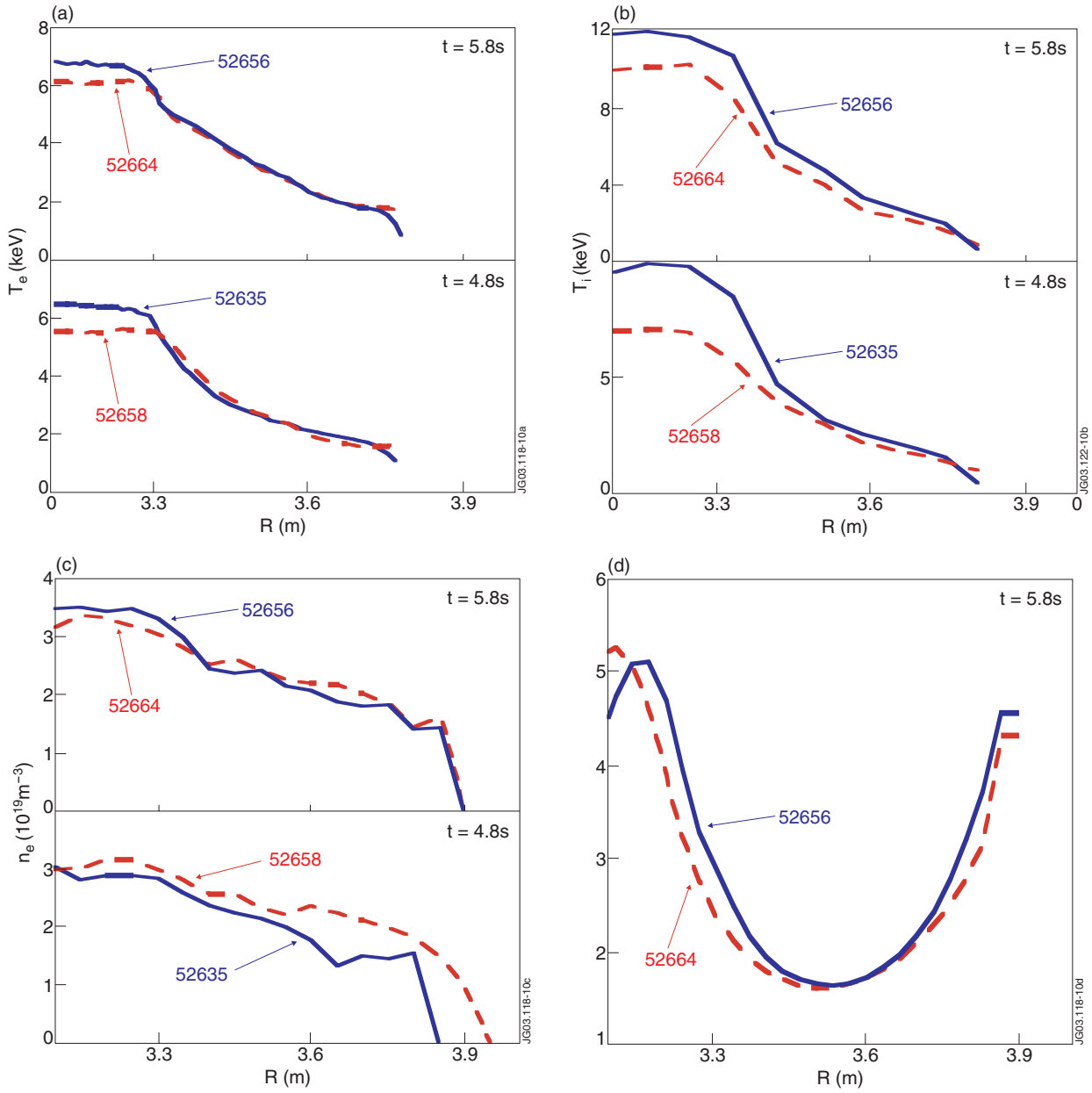

Fig.10: Radial profiles, at fixed time, for some quantities of two couples of discharges similar in all the parameters, but the elongation. #52664, #52658 (LD-LK) and #52656, #52635 (LD-HK) a) Electron temperature; b) ion temperature; c) electron density; d) q_ψ.

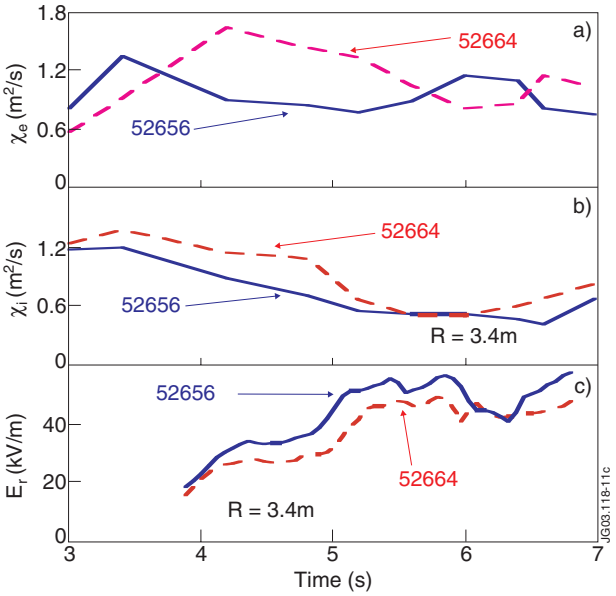

Fig.11: Time evolution, at the ITB radius, of the electron (χ_e - a) ion (χ_i - b) thermal conductivity and of the radial electric field E_r (c) for the two discharges #52656 (LD-HK) and #52664 (LD-LK).